An Optimized Image Matching Method for Determining In-Vivo TKA Kinematics with a Dual-Orthogonal Fluoroscopic Imaging System

Jeffrey Bingham
Bioengineering Laboratory,
Department of Orthopaedic Surgery,
Massachusetts General Hospital/Harvard
Medical School
and Department of Mechanical Engineering,
Massachusetts Institute of Technology,
Boston, MA

Guoan Li[1]
Bioengineering Laboratory,
Department of Orthopaedic Surgery,
Massachusetts General Hospital/Harvard
Medical School,
Boston, MA
e-mail: gli1@partners.org

This study presents an optimized matching algorithm for a dual-orthogonal fluoroscopic image system used to determine six degrees-of-freedom total knee arthroplasty (TKA) kinematics in-vivo. The algorithm was evaluated using controlled conditions and standard geometries. Results of the validation demonstrate the algorithm's robustness and capability of realizing a pose from a variety of initial poses. Under idealized conditions, poses of a TKA system were recreated to within 0.02±0.01 mm and 0.02±0.03 deg for the femoral component and 0.07±0.09 mm and 0.16±0.18 deg for the tibial component. By employing a standardized geometry with spheres, the translational accuracy and repeatability under actual conditions was found to be 0.01±0.06 mm. Application of the optimized matching algorithm to a TKA patient showed that the pose of in-vivo TKA components can be repeatedly located, with standard deviations less than ±0.12 mm and ±0.12 deg for the femoral component and ±0.29 mm and ±0.25 deg for the tibial component. This methodology presents a useful tool that can be readily applied to the investigation of in-vivo motion of TKA kinematics. [DOI: 10.1115/1.2205865]

Introduction

Fluoroscopic imaging techniques have been used extensively to measure in-vivo kinematics of total knee arthroplasty (TKA) because of the relatively low radiation dosage and the accessibility of the equipment [1–3]. Previous studies employed a single fluoroscope to take sagittal plane images of the knee at multiple flexion angles [1,4–7]. Using the geometry of the fluoroscope, three-dimensional (3D) computer models of the tibial and femoral components were matched to the two-dimensional (2D) features of the acquired fluoroscopic images. When the features were considered to be matched, the relative poses of the 3D component models represented the in-vivo knee kinematics, where pose is defined as the position and orientation specifying the six degree-of-freedom (6DOF) location of an object. Using this technique numerous data have been reported on knee motion within the image plane of the fluoroscope. However, determining knee motion in the direction perpendicular to the fluoroscopic image plane has been questioned in recent studies [8–10].

Pursuing higher accuracies with fluoroscopy, Li et al. [10] completed a 3D study on quasi-dynamic in-vivo kinematics of the knee and more recently, Hanson et al. [2] and Suggs et al. [11] applied two fluoroscopes to formulate a dual-orthogonal fluoroscopic system to investigate in-vivo TKA kinematics. These studies utilized a computer aided drafting (CAD) program to simulate the fluoroscopic environment and manually manipulate 3D TKA models in space so that their projected silhouettes matched outlines of the components on both fluoroscopic images. This methodology has been proven to accurately recreate the 6DOF motion of the knee at multiple flexion angles [2]. However, the manual matching procedure is laborious, impairing its application to study continuous dynamic motion. Automating the matching procedure would reduce the time required to match and improve the repeatability of the dual fluoroscope methodology in determining in-vivo TKA kinematics.

In this paper, an optimization algorithm is presented for automating the process of matching projections of 3D TKA CAD models of tibial and femoral components to two orthogonal planar images of TKA components acquired with a dual-orthogonal fluoroscopic imaging system. Accuracy and repeatability of the algorithm's ability to determine 6DOF location of TKA components are discussed. Results from the validation demonstrate the repeatability of the algorithm for determining in-vivo TKA poses.

Methods

Dual-Orthogonal Fluoroscopic System. The dual-orthogonal fluoroscopic image system consists of two fluoroscopes (OEC® 9800 ESP, GE, Salt Lake City) positioned with the two image intensifiers perpendicular to each other [2] (Fig. 1). A subject is free to move within the common imaging zone of the two fluoroscopes. The subject is then asked to move through a series of flexion angles which are imaged simultaneously by the fluoroscopes to acquire images of the knee from two perpendicular directions. During this procedure, the average subject receives 106 mrem of radiation for 20 sec of pulsed fluoroscopy at 65 kVp and 0.80 mA. In addition to the subject images, a set of calibration images are acquired. Calibration images are taken of a perforated plate for distortion correction and a set of beads in a known configuration for the recreation of the fluoroscopic geometry. The images are stored electronically with an 8-bit grey scale and a resolution of 1024×1024 pixels, corresponding to a 315×315 mm field of view. This procedure records the in-vivo poses of the knee as a series of 2D paired orthogonal fluoroscopic images.

The images are then automatically segmented using Canny edge detection [12]. Next, the segmented fluoroscopic images are corrected for distortion using the method of Gronenschild [13].

[1]Corresponding author. Bioengineering Laboratory, MGH/Harvard Medical School, 55 Fruit St., GRJ 1215, Boston, MA 02114.

Contributed by the Bioengineering Division of ASME for publication in the JOURNAL OF BIOMECHANICAL ENGINEERING. Manuscript received June 10, 2005; final manuscript received January 6, 2006. Review conducted by Jeffrey A. Weiss.

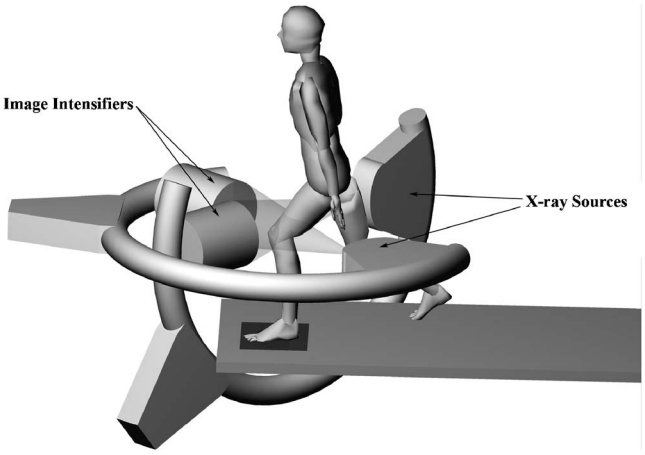

Fig. 1 A dual-orthogonal fluoroscopic system for capturing in-vivo knee joint kinematics

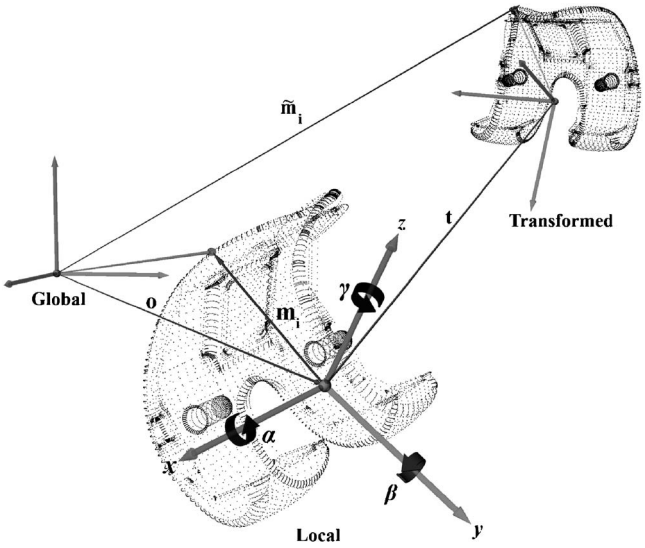

Fig. 3 Definition of local and global coordinate systems and the transformation of model points

The outlines of the TKA components from the edge detection are manually reviewed and saved as a list of 2D spatial points. The point outlines from the segmented fluoroscopic images of the TKA components are used to create spline curves, using a periodic spline algorithm [14]. The starting and ending values of the newly created splines are recorded for determining the valid limits of the splines. These algorithms are implemented using functions in the MATLAB® software (Matlab v7r14, Mathworks, Natick, MA).

Next, a virtual replica of the dual-orthogonal fluoroscopic system is constructed. Using calibration data, two virtual source-intensifier pairs are created in a solid modeling program (Rhinoceros®, Robert McNeel & Associates, Seattle, WA). Then, the virtual intensifiers are oriented so that their relative locations replicate the geometry of the real fluoroscopic system (Fig. 2).

The splines of the TKA components obtained from the dual fluoroscopic images are placed on their respective virtual intensifiers. Next, 3D CAD models of the TKA tibial and femoral components are introduced into the virtual system. The TKA models are obtained from the manufacturer as nonuniform rational b-splines (NURBS) surfaces. Using the 3D modeling program a mesh size is selected. The surfaces are tessellated, and the vertices of the mesh are used to create a 3D point cloud of the model. Then, a local coordinate system is created for each point model. The local coordinate system is related to the global coordinates of the virtual fluoroscopic environment using a position vector and rotation matrix (Fig. 3). Using the 3D modeling program the point model can be manipulated in the virtual environment to create an initial guess of the TKA pose. With this CAD replica a mathematical model of the dual-orthogonal fluoroscopic system is constructed and matching can commence.

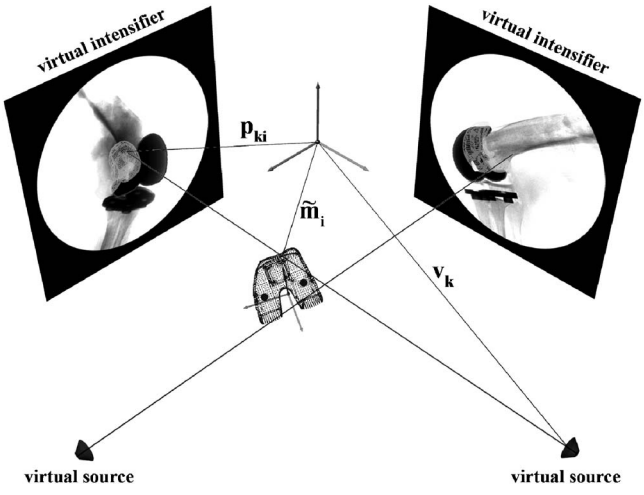

Fig. 2 A virtual dual-orthogonal fluoroscopic system constructed to reproduce the in-vivo knee joint kinematics

Optimized Matching Algorithm. The optimized matching algorithm is formulated as an optimization procedure that minimizes the error between projected model silhouettes and actual fluoroscopic image outlines in order to determine the model pose. The model pose is defined by the 6DOF position and orientation of each model's local coordinate system relative to the global coordinate system. The objective function is expressed as a scalar function with six independent variables. The independent variables are the three components of the position vector locating the origin of the local coordinate system and the three Euler angles of the local system in the global system (Fig. 3). The scalar function value is the average distance between the 3D projected model silhouettes and the segmented fluoroscopic outlines.

Transformation of Model Points. The six independent variables are used to transform the points of the 3D model from an initial pose to a new position and orientation which is illustrated in Fig. 3. Each point on the model, noted as m_i, is transformed with the local coordinate system to a new location and orientation in the global coordinate system, noted as $\tilde{\mathbf{m}}_i$ (Eq. (1)).

$$\tilde{\mathbf{m}}_i = \mathbf{R}(\mathbf{m}_i) + (\mathbf{t} + \mathbf{o}) \tag{1}$$

The vector $\mathbf{o}=\{o^x, o^y, o^z\}$ locates the origin of the local system in the global coordinates. The translation vector $\mathbf{t}=\{x, y, z\}$ is defined in the global coordinate system. The rotation matrix $\mathbf{R}$ is defined as a *Y-Z-X* Euler sequence using the angles α, β, and γ (Eq. (2)).

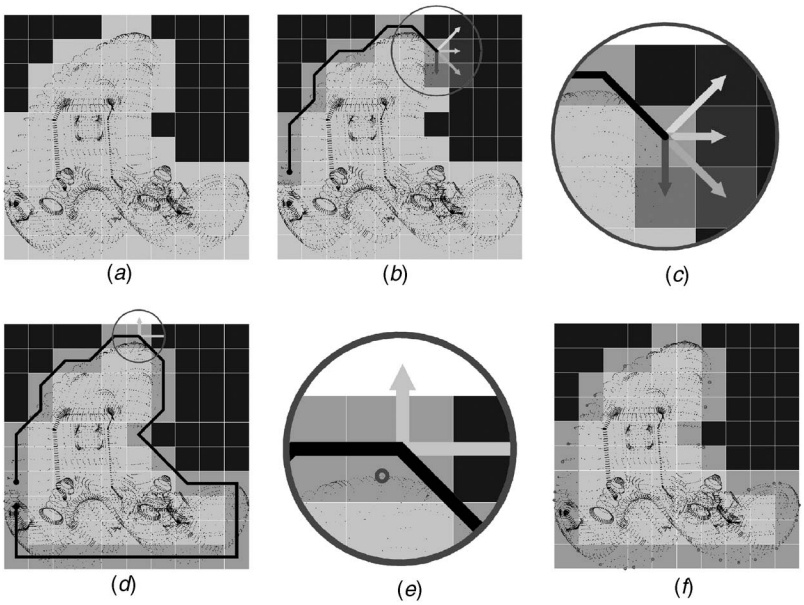

Fig. 4 Outlining procedure. (a) Compartmentalize projected points (b) and (c) determine boundary grids with left-looking outlining technique (d) and (e) select point in each grid that is closest to the outer edge. (f) Completion of algorithm with selected outline points.

$$\mathbf{R} = \begin{bmatrix} \cos\beta\cos\gamma & \sin\gamma & -\sin\beta\cos\gamma \\ -\cos\alpha\cos\beta\sin\gamma+\sin\alpha\sin\beta & \cos\alpha\cos\gamma & \cos\alpha\sin\beta\sin\gamma+\sin\alpha\cos\beta \\ \sin\alpha\cos\beta\sin\gamma+\cos\alpha\cos\beta & -\sin\alpha\cos\gamma & -\sin\alpha\sin\beta\sin\gamma+\cos\alpha\cos\beta \end{bmatrix} \tag{2}$$

Once the 3D model is transformed to a new pose, the locations of the virtual sources are used to project the points onto the intensifiers of the virtual fluoroscopic system (Fig. 2). The vector equation used to project the transformed 3D model points onto a virtual intensifier is shown below (Eq. (3)).

$$\mathbf{p}_{ki} = \mathbf{v}_k + \frac{l_k}{(\tilde{\mathbf{m}}_i - \mathbf{v}_k)\cdot\mathbf{n}_k}(\tilde{\mathbf{m}}_i - \mathbf{v}_k) \tag{3}$$

The ith projected model point for the kth intensifier is defined as p_{ki} and $\tilde{\mathbf{m}}_i$ the ith transformed model point. The vector $\mathbf{v}_k$ locates the kth source and $\mathbf{n}_k$ the unit vector normal to the kth intensifier plane. The scalar l_k is the distance between the kth source and intensifier.

Calculation of Performance Index. To decrease computation time and improve the robustness of the algorithm, only the outline points of the projected 3D model points are compared to the outlines of the TKA components. An outlining set of the projected points is determined by establishing point connectivity and following an outer contour defined by the connectivity. Connectivity is determined by automatically compartmentalizing the model points so that a connected grid is produced (Fig. 4(*a*)). Using a left-looking, contour-following algorithm, the grids that outline the projected points are determined (Figs. 4(*b*) and 4(*c*)). For each contour grid, the point closest to the outside of the contour is selected (Figs. 4(*d*) and 4(*e*)). This automatic procedure results in a set of points that form an outline of the projected 3D model points (Fig. 4(*f*)).

Next, the minimum distance between each outlined, projected 3D model point and the fluoroscopic spline is determined (Fig. 5). Since the spline is represented as a parametric curve, the secant method is used to determine the minimum distance between a point and the spline (Eq. 4).

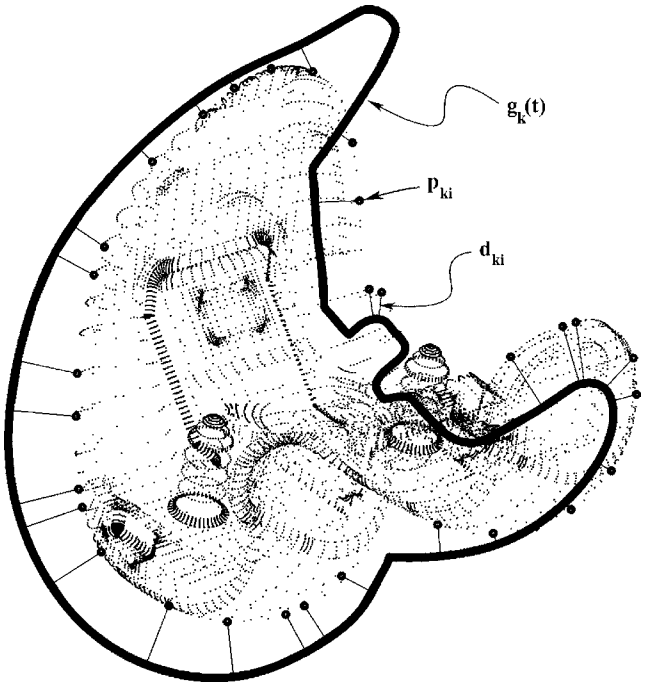

Fig. 5 Representation of calculating the minimum distance between projected points and a fluoroscopic outline

$$d_{ki} = \min_t |\mathbf{g}_k(t) - \mathbf{p}_{ki}| \tag{4}$$

For the kth intensifier, d_{ki} is the ith minimum distance, $\mathbf{p}_{ki}$ is the ith projected model point, $\mathbf{g}_k(t)$ is the parametric vector function of the fluoroscopic image spline, and $\mathbf{t}$ is the parametric variable, whose range corresponds to the recorded endpoints of the spline. For each intensifier, these distances are summed and divided by the total number of points q_k resulting in a normalized distance. The normalized distances for each intensifier are then summed and returned as the value of the objective function, I (Eq. (5)).

$$\begin{aligned} I &= \sum_{k=1}^{2} \frac{1}{q_k} \sum_{i=1}^{q_k} d_{ki} \\ &= \sum_{k=1}^{2} \frac{1}{q_k} \sum_{i=1}^{q_k} \left[\min_t \left| \mathbf{g}_k(t) - \mathbf{v}_k - \frac{l_k[\mathbf{R}(\mathbf{m}_i) + (\mathbf{t} + \mathbf{o}) - \mathbf{v}_k]}{\mathbf{n}_k \bullet (\mathbf{R}(m_i) + (\mathbf{t} + \mathbf{o}) - \mathbf{v}_k)} \right| \right] \end{aligned} \tag{5}$$

Optimization. As the objective function I approaches zero the 3D model closely approaches the actual TKA pose. Therefore, to accurately replicate the actual TKA pose the objective function is minimized according to Eq. (6).

$$J = \min_{(x,y,z,\alpha,\beta,\gamma)} I \tag{6}$$

The six optimization variables $(x, y, z, \alpha, \beta, \gamma)$ represent the position and orientation of the model's local coordinate system with respect to the global coordinate system. Minimization of this function is accomplished with the Broyden, Fletcher, Goldfarb, and Shanno (BFGS) quasi-Newton method [15] and implemented in MATLAB® software. Convergence is controlled by terminating the minimization routine when the differential change in variables meets the required tolerance or the quantity of objective function calls exceeds a specified number. Therefore, runs that exceed the number of function calls and do not meet the required tolerance are deemed non-convergent in this study.

VALIDATION

The algorithms presented in this paper were implemented on a personal computer with a Pentium IV® class processor (2.4 GHz, 512 MB RAM) running the Microsoft Windows XP Professional® operating system. Using this same computer system, a validation of the optimized matching algorithm was performed to demonstrate the accuracy and repeatability of recreating the TKA pose. Validation consisted of running the algorithm with idealized, controlled, and real data using ten randomly generated initial pose estimates for each test. These tests were used to isolate various causes of error; idealized tests to isolate errors with geometry, standardized tests to isolate errors caused by segmentation, and in-vivo tests to observe the combination of errors. For all tests the matching algorithm was set to record convergent solutions that did not exceed 800 objective function calls and had a differential tolerance of less than 0.0005 for each variable.

Idealized Testing. An idealized environment was created in order to determine the optimized matching algorithm's repeatability, accuracy, sensitivity to model point density and pose orientation, and optimal parameters under controlled conditions. These tests gave a basis for the ultimate potential of the algorithm. The idealized fluoroscopic setup was created by replicating the fluoroscopic environment using the 3D solid modeling software. Three-dimensional TKA models from the manufacturer were oriented in the system in poses approximating a deep knee bend. From these poses the models were projected onto the virtual intensifiers, and the projections were used to create pseudo fluoroscopic outlines.

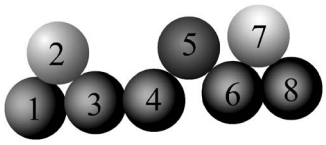

Fig. 6 Geometry of standardized test. Spheres two and seven were ceramic, sphere five was tungsten, and the remaining spheres were stainless steel. The spheres were stacked in the vertical plane.

Models in this configuration were then considered to be the gold standard. The error of the matched poses was then determined by comparing the matched model poses to the gold standards.

With the idealized fluoroscopic setup the effect of model point density was tested for one pose of the tibial and femoral components (45 deg flexion position) using three different densities. The low point density models used a coarse mesh with approximately 3500 points. Medium density point models were approximately 15,000 points and high density point models were made with over 20,000 points. Three additional poses (30 deg, 60 deg and 90 deg flexion positions) for the medium point density models were matched to test the effect of pose orientation. For each pose ten estimates for the initial guess were created for each component by perturbing the models from the gold standard. The perturbations were created by randomly generating values for the pose variables within the range of ±20 mm and ±20 deg using a Gaussian distribution. Next, the models were matched using 50 of the projected outline points. The accuracy and repeatability of the optimized matching algorithm in reproducing the femoral and tibial components position and orientation in 6DOF was recorded for each convergent match.

Standardized Testing. To determine accuracy and repeatability of the optimized matching algorithm when subjected to actual conditions, a standardized test in the manner of Short et al. was performed [16]. The test consisted of eight spheres 12.70 mm in diameter each having a tolerance of ±0.01 mm. Five of the spheres were stainless steel, two were ceramic (spheres 2 and 7), and one was tungsten (sphere 5). The spheres were arranged in a fixed pattern (Fig. 6) and imaged with the dual-orthogonal fluoroscopic system.

Using the solid modeling program a spherical model 12.70 mm in diameter was created and converted into a point cloud containing 2500 points. Next, the model was placed centrally in the virtual fluoroscopic environment. Then, ten estimates for the initial pose were created for each component by perturbing the model from the placed configuration. The perturbations were created by randomly generating values for the pose variables within the range of ±20 mm using a Gaussian distribution. Next, the models were matched using 60 of the projected outline points and the convergent matches were recorded. The accuracy of the matching algorithm was determined by comparing the distance between the adjacent matched spheres and the true distance of one diameter, 12.70 mm.

Application to In-Vivo Total Knee Arthroplasty (TKA) Kinematics. The final test employed in-vivo images taken with the dual fluoroscopic system of the right knee of a patient after TKA. The images were acquired under Internal Review Board (IRB) approval and with informed consent of the patient. The patient had a cruciate retaining component and images were taken during a lunge (NexGen CR TKA, Zimmer, Inc, Warsaw). Poses selected for matching were for images taken at 10 deg and 50 deg of flexion of the patient.

Using the solid modeling program the component models were converted into point clouds containing 15,000 points. Next, the models were manually matched to the fluoroscopic contours in the virtual fluoroscopic environment. Then, for both flexion angles

Table 1 Accuracy (average error values), repeatability (standard deviations), and root-mean-square errors (RMSE) of the automatic matching procedure in an idealized environment using different model point densities. Accuracy and repeatability were evaluated for ten initial positions.

	Error in femoral component pose parameters (Avg±Std Dev [RMSE])					
	Translation (mm)			Rotation (deg)		
Model size	Δx	Δy	Δz	$\Delta\alpha$	$\Delta\beta$	$\Delta\varphi$
3477	−0.001±0.016 [0.016]	−0.006±0.037 [0.041]	−0.009±0.021 [0.030]	0.007±0.030 [0.040]	−0.050±0.099 [0.197]	−0.038±0.160 [0.413]
14135	0.002±0.005 [0.014]	−0.002±0.006 [0.006]	−0.018±0.012 [0.021]	0.004±0.004 [0.019]	−0.017±0.020 [0.057]	0.015±0.019 [0.086]
21224	0.009±0.006 [0.024]	−0.023±0.009 [0.041]	−0.005±0.003 [0.007]	0.002±0.008 [0.011]	0.068±0.006 [0.102]	−0.029±0.008 [0.047]
	Error in tibial component pose parameters (Avg±Std Dev [RMSE])					
	Translation (mm)			Rotation (deg)		
Model size	Δx	Δy	Δz	$\Delta\alpha$	$\Delta\beta$	$\Delta\varphi$
3608	−0.283±0.304 [0.403]	0.044±0.068 [0.078]	0.004±0.013 [0.013]	0.088±0.062 [0.106]	−0.079±0.051 [0.092]	−0.747±0.706 [1.001]
14505	−0.069±0.043 [0.080]	0.029±0.018 [0.033]	−0.009±0.003 [0.010]	−0.163±0.080 [0.180]	−0.042±0.036 [0.054]	0.069±0.102 [0.118]
35994	−0.049±0.018 [0.051]	0.016±0.009 [0.018]	−0.011±0.003 [0.012]	−0.074±0.010 [0.075]	−0.011±0.010 [0.014]	−0.189±0.104 [0.213]

each model was perturbed ten times to create estimates of the initial pose. The perturbations were created by randomly generating values for the pose variables within the range of ±20 mm and ±20 deg using a Gaussian distribution. Sixty projected outline points were used for the matches and the convergent solutions were recorded. Since the accurate position and orientation of the patient TKA is unknown, this test was designed to evaluate repeatability of the algorithm in determining the position and orientation of in-vivo TKA components.

Results

Idealized Testing. Accuracy for the idealized tests was measured as the error between the body fixed local coordinate systems of the golden standard and the matched models. The sample standard deviation of these errors was selected as the measure of repeatability. Root-mean-square error (RMSE), or population standard deviation, values are also reported for comparison with previous methods. Results for different densities of the femoral component are presented in Table 1. The pose of the femoral component was recreated to within 0.01 mm±0.04 mm in translation and 0.05 deg±0.16 deg in rotation for the low point density model, 0.02 mm±0.01 mm and 0.02 deg±0.02 deg for the medium point density model, and 0.02 mm±0.01 mm and 0.07 deg±0.01 deg for the high point density model. The average time for matching a single pose was 200, 350, and 510 sec for the low, medium, and high point density models, respectively. The average number of calls to the objective function was 640 for all model sizes. The results for four different flexion angles using the medium point density model are listed in Table 2. The average values of the pose variables were found to recreate pose to within 0.02 mm±0.01 mm in translation and 0.02 deg±0.03 deg in rotation.

Results for the tibial component are presented in Table 1 for different densities of the model. Pose was recreated to within 0.28 mm±0.30 mm in translation and 0.75 deg±0.71 deg in rotation for the low density model, 0.07 mm±0.04 mm and 0.16 deg±0.10 deg for the medium point density model, and 0.05 mm±0.02 mm and 0.19 deg±0.10 deg for the high point

Table 2 Accuracy (average error values), repeatability (standard deviations), and root-mean-square errors (RMSE) of the automatic matching procedure in an idealized environment using four different pose environments with a model point density of 15,000 points. Each position was evaluated for ten initial positions.

	Error in femoral component pose parameters (Avg±Std Dev [RMSE])					
	Translation (mm)			Rotation (deg)		
Position	Δx	Δy	Δz	$\Delta\alpha$	$\Delta\beta$	$\Delta\varphi$
1	0.002±0.005 [0.014]	−0.002±0.006 [0.006]	−0.018±0.012 [0.021]	0.004±0.004 [0.019]	−0.017±0.020 [0.057]	0.015±0.019 [0.086]
2	−0.003±0.010 [0.010]	−0.010±0.009 [0.013]	−0.004±0.008 [0.008]	0.005±0.025 [0.023]	0.001±0.008 [0.007]	−0.008±0.011 [0.012]
3	−0.000±0.009 [0.008]	0.001±0.014 [0.012]	−0.001±0.005 [0.004]	0.005±0.011 [0.012]	−0.003±0.021 [0.019]	−0.009±0.023 [0.023]
4	−0.006±0.011 [0.011]	−0.002±0.010 [0.009]	0.000±0.007 [0.006]	−0.013±0.023 [0.025]	0.009±0.018 [0.018]	−0.001±0.027 [0.024]
	Error in tibial component pose parameters (Avg±Std Dev [RMSE])					
	Translation (mm)			Rotation (deg)		
Position	Δx	Δy	Δz	$\Delta\alpha$	$\Delta\beta$	$\Delta\varphi$
1	−0.069±0.043 [0.080]	0.029±0.018 [0.033]	−0.009±0.003 [0.010]	−0.163±0.080 [0.180]	−0.042±0.036 [0.054]	0.069±0.102 [0.118]
2	−0.013±0.032 [0.033]	0.005±0.024 [0.024]	−0.001±0.011 [0.010]	0.003±0.012 [0.012]	−0.005±0.019 [0.019]	−0.020±0.084 [0.083]
3	−0.010±0.057 [0.056]	0.010±0.170 [0.164]	0.013±0.034 [0.035]	−0.009±0.023 [0.024]	0.011±0.043 [0.043]	−0.042±0.138 [0.139]
4	0.012±0.096 [0.092]	−0.008±0.041 [0.039]	0.003±0.025 [0.024]	−0.004±0.051 [0.048]	−0.013±0.041 [0.041]	0.163±0.389 [0.403]

Table 3 Standardized test validating accuracy and precision of the dual-orthogonal fluoroscopic system under actual conditions with spheres of different materials using ten initial positions

Error in separation distance of spheres (Avg±Std Dev [RMSE])	
Sphere pairs	Distance (mm)
1 to 2	12.76±0.04 [0.07]
2 to 3	12.72±0.03 [0.03]
3 to 4	12.56±0.01 [0.14]
4 to 5	12.72±0.02 [0.03]
5 to 6	12.66±0.04 [0.06]
6 to 7	12.75±0.06 [0.07]
7 to 8	12.68±0.05 [0.06]
Mean	12.69
Std. Dev.	±0.06
RMSE	0.06

density model. The average time for matching a single pose was 110, 210, and 220 sec for the low, medium, and high point density models, respectively. For each model size the average number of objective function calls was 650. Results from four different flexion angles for the medium point density model are listed in Table 2. The average values of the pose variables were found to recreate pose to within 0.07 mm±0.09 mm in translation and 0.16 deg±0.18 deg in rotation for the tibial component.

Standardized Testing. For the standardized test, the distance between each adjacent pair of spheres was calculated (Table 3). A maximum distance of 12.76 mm was calculated between spheres 1 and 2 and a minimum distance of 12.56 mm was calculated between spheres 5 and 6. The average distance between matched pairs of adjacent spheres was 12.69 mm, 0.01 mm less than the actual distance data, with a standard deviation of 0.06 mm. The average time for each match of a single sphere was 15 sec with 380 calls to the objective function.

Application to In-Vivo TKA Kinematics. This in-vivo application demonstrated the repeatability of the method by comparing the variation of matched models when different initial guesses were used in the optimization procedure. Results are tabulated for two poses of both the tibial and femoral components in Table 4. Maximum translational deviation for both poses was ±0.12 mm for the femoral component and ±0.29 mm for the tibial component. Maximum angular deviation for both poses was ±0.12 deg for the femoral component and ±0.25 deg for the tibial component. The average time to match a single pose for each component was 500 sec with 600 calls to the objective function.

Table 4 Repeatability of the automatic matching procedure in reproducing the two in-vivo poses of the femoral and tibial components of a TKA patient for ten initial positions

Error in femoral component pose parameters (Std Dev)						
	Translation (mm)			Rotation (deg)		
Position	Δx	Δy	Δz	$\Delta\alpha$	$\Delta\beta$	$\Delta\varphi$
1	0.018	0.016	0.086	0.050	0.086	0.019
2	0.038	0.010	0.116	0.117	0.087	0.017
Error in tibial component pose parameters (Std Dev)						
	Translation (mm)			Rotation (deg)		
Position	Δx	Δy	Δz	$\Delta\alpha$	$\Delta\beta$	$\Delta\varphi$
1	0.106	0.294	0.042	0.218	0.109	0.070
2	0.124	0.270	0.031	0.250	0.067	0.068

Discussion

Fluoroscopic techniques have been used extensively in recent years for determining in-vivo TKA kinematics [1,7,9,17]. These techniques offer advantages over roentgen stereo-photogrammetry (RSA) and conventional x-ray because of the reduced radiation exposure and noninvasive methods. In the pursuit of improved accuracy using fluoroscopy, recent studies have developed a dual-orthogonal fluoroscopic system for determining 6DOF TKA [2] and normal knee kinematics when combined with magnetic resonance MR image-based 3D knee models [18,19]. These methods have been shown to be accurate using a manual process [10,20], but for investigation of joint motion, which requires many fluoroscopic images, an optimized image matching process is desired. This paper developed an optimized image matching algorithm for determining 6DOF poses of TKA components using the dual-orthogonal fluoroscopic system. The optimized matching procedure was evaluated using idealized, standardized, and in-vivo test environments.

Idealized testing gave an empirical measure of the accuracy of the optimized matching algorithm and provided a controlled environment for examining the optimal point model density, number of matching points, and effect of initial poses. Results showed that increasing the model point density improved repeatability; however, accuracy remained roughly constant. Point density affects the sensitivity of rotational accuracy more than positional accuracy. For this reason model point density has a greater effect on the "axis-symmetric" tibial component. Since calculation time increases roughly linearly and error decreases quadratically, the point of diminishing returns for accuracy and repeatability of matching femoral and tibial components occurs at approximately 15,000 model points. In general, the optimal model point density occurs when the entire model surface is covered with an evenly distributed number of points that accurately capture the geometry.

The number of projected outline points used for matching affects the robustness of the matching algorithm and is dependent on model geometry. The optimal number of points should be sufficient to characterize a given projection geometry. However, characteristic points are difficult to define automatically. A simple method for circumventing manual placement is to automatically select a set of equally spaced points. Experience has shown that selecting a point every 4 mm on the projected outline of TKA components adequately captures the geometric character. Interestingly, using large numbers of outline points does not significantly improve accuracy; however, fewer iterations are required for convergence.

The idealized testing environment also determined the effect of initial pose estimates on resulting component pose. It was found that perturbations within the range of 1–20 mm and 0.5–20 deg from the ideal position and orientation resulted in similar results for a range of model orientations. These data showed that the optimized matching process is forgiving of the initial pose estimate and allows for minimal operator intervention.

Standardized testing allowed for evaluating the accuracy and repeatability of the optimized matching procedure with the actual dual-orthogonal fluoroscopic system. Standardized geometries allowed for known relative poses, which is difficult to achieve using actual TKA components. Different materials for the spheres were used to simulate possible edge loss from overexposure and edge blooming from x-ray scatter due to differences in material density. In addition, cases of occlusion were also present, because of the geometry of the spheres. These image artifacts caused incorrect or incomplete segmentation of the fluoroscopic images; however, most artifacts were not severe in both views and the combined information of the two orthogonal views reduced the difficulty of matching. The results of these tests showed that the accuracy and repeatability for the standardized and idealized tests had similar orders of magnitude and that the different materials did not disrupt the optimized matching algorithm's ability to recreate the spheres' pose. Furthermore, noise, occlusion, and distortion may affect the

quality of the edges, but due to the geometry of the imaging system and "fitting" nature of the algorithm, these errors are often obviated. Edge quality is of greater concern when imaging natural joints and soft tissue; however, the positive results of this study allude to the possibility that this optimization method could be applied to in-vivo kinematics of intact knees with further validation.

To prove the capabilities of the optimized matching algorithm for use with TKA kinematics, the method was applied to an actual TKA patient. The data demonstrated that the optimized matching procedure was highly repeatable when different initial guesses were used. Repeatability for the femoral component was better than the tibial component because of the symmetry of the tibial component. This phenomenon was also observed in the idealized testing (Table 1). Symmetric objects are more difficult to match than objects of irregular geometry because of the reduced sensitivity in the projected silhouette. As sensitivity decreases, the optimization routine is less likely to converge.

The results of this validation compare favorably to previous fluoroscopic methods which have employed a variety of techniques for determining the pose of 3D objects from 2D images. These methods can be broadly grouped into either template matching [1,4] or hypothesize and test methods [21]. Template matching techniques compare segmented outlines from fluoroscopic outlines to a library of previously calculated silhouettes of component models. Hypothesize and test methods first "hypothesize" a location and orientation of a model, and then test the validity of the pose based on fluoroscopic images.

Template matching techniques were implemented in early works by Banks and Hodge [1] and Hoff et al. [4]. With the evolution of computing power these techniques have recently been eclipsed by hypothesize and test methods. Hypothesize and test methods can be further classified based on the type of "test." The most common tests are iterative closest point (ICP) [6,22], iterative inverse point (IIP) [7,17,23], and digitally reconstructed radiograph (DRR) [8,16,24]. The ICP method minimizes the distance between projected model points and points on the fluoroscopic outlines. IIP methods minimize the distance between a model's surface and the rays connecting points on the fluoroscopic outline to the virtual x-ray source. DRR methods use ray-tracing algorithms to render simulated fluoroscopic images of TKA components and correlate the intensity values of the pixels and matching of segmented features to the actual fluoroscopic images.

IIP and DRR methods are significantly more complex than ICP algorithms, but are gaining ground due to the recent advances in computing power and accessibility of high-power graphics software. ICP and IPP methods may be more susceptible to segmentation errors [25], but provide a more stable optimization problem than DRR methods.

It should be noted that single plane implementation of these methods are limited in their accuracy for determining accurate 6DOF TKA kinematics because of the discrepancy between in-plane and out-of-plane accuracy. A recent parametric analysis of single imaging techniques showed that for a desired accuracy in the out-of-plane direction, the in-plane accuracy needed to be at least an order of magnitude better [2,10]. Another recent article by Garling et al. illustrated that with an in-plane accuracy of less than 0.17 mm in translation out-of-plane error could reach 1.9 mm [22]. Other studies using single fluoroscopic techniques have also reported similar results [1,6,17,24].

In order to improve on previous methods, this study implemented a modified ICP method that matches projected model points to spline curves on two orthogonal image intensifiers. Using a dual-orthogonal fluoroscopic system significantly improves accuracy over single fluoroscopic systems. This is because out-of-plane errors of one fluoroscope are the in-plane errors of the other fluoroscope. In addition, the use of two orthogonal contours for matching significantly amplifies the global minima and the use of splines smoothes the matching space, thus improving algorithm convergence. Results from this study confirm statements from similar studies that the use of dual-orthogonal fluoroscopy can dramatically enhance accuracy for true submillimeter accuracy of in-vivo TKA kinematics in 6DOF [8,16,20,26–28]. Run times are also favorable at around four to eight minutes and compare with similar methods [8,23,26].

It is important to state that using dual images is not new. Marker and model based RSA, which use two x-ray beams, has been used to determine knee, ankle, and shoulder kinematics [8,16,29]. Application of two x rays has also been used to determine normal knee kinematics combined with CT image-based knee models [8,20,27,28]. Not surprisingly, these studies presented accuracies similar to the dual-orthogonal fluoroscopic methodology. However, the higher radiation doses, stationary equipment, and limited field of view associated with conventional x-ray present difficulties when determining in-vivo TKA motion. The dual-orthogonal fluoroscopic technique bridges the accuracy of RSA and the minimal invasiveness of fluoroscopy, to bring together the best attributes of both methods. This synergy produces an improved tool for investigating joint kinematics. Combining the dual-orthogonal fluoroscopic system with the optimized image matching procedure developed in this paper provides a powerful tool for processing large quantities of image sets rapidly.

There are a few limitations with the validation studies presented in this paper. In the absence of an in-vivo gold standard pose, we applied alternative tests to evaluate the accuracy and repeatability of the optimization algorithm. The idealized case only tested the geometric factors; it did not consider the possible effects of image quality. The standardized test accounted for the effect of image quality, but it did not represent the complicated geometries of TKA components. Finally, the application to in-vivo TKA patient data did not indicate the accuracy of the optimization method when used under in-vivo conditions; rather, it showed the consistency of the results on 6DOF TKA kinematics when different initial guesses were used in the optimization procedure. In the future, when a gold standard for TKA positions under in-vivo conditions becomes available, the validation of this method can be improved for any applications that are aimed at determining 6DOF TKA kinematics.

In conclusion, this study presents an optimized matching procedure for a dual-orthogonal fluoroscopic image system to determine 6DOF TKA kinematics in vivo. The method was validated using controlled conditions and standard geometries. The method has been shown to be robust and capable of realizing a pose from a variety of initial poses accurately. Furthermore, application of the optimized matching procedure to a TKA patient shows that the pose of in-vivo TKA components can be repeatedly located. This methodology could be a useful tool for investigating in-vivo TKA kinematics and with further research could be readily applied to the investigation of in-vivo motion of other joints, such as the elbow, shoulder, and ankle.

Acknowledgment

We thank George Hanson, Jeremy Suggs, Louis DeFrate, Lu Wan, and Ramprasad Papannagari of the MGH Bioengineering Laboratory for their technical assistance. This work was partially supported by NIH R01 AR052408.

References

[1] Banks, S. A., and Hodge, W. A. 1996, "Accurate Measurement of Three-Dimensional Knee Replacement Kinematics Using Single-Plane Fluoroscopy," IEEE Trans. Biomed. Eng., **43**(6), pp. 638–649.

[2] Hanson, G., Suggs, J., Freiberg, A., Durbhakula, S., and Li, G., 2006 "Investigation of In Vivo 6dof Total Knee Arthroplasty Kinematics Using a Dual Orthogonal Fluoroscopic System," J. Orthop. Res., **24**(5), pp. 974–981.

[3] Stiehl, J., Komistek, R., Dennis, D., Paxson, R., and Hoff, W., 1995 "Fluoroscopic Analysis of Kinematics After Posterior-Cruciate-Retaining Knee Arthroplasty," J. Bone Jt. Surg., Br. Vol. **77B**(6) pp. 884–889.

[4] Hoff, W., Komistek, R., Dennis, D., Walker, S., Northcut, E., and Spargo, K., 1996, "Pose Estimation of Artificial Knee Implants in Fluoroscopy Images Using a Template Matching Technique," *Proceedings of the Third IEEE Work-*

shop on Applications of Computer Vision, 2–4 Dec., Sarasota, FL, IEEE, pp. 181–186.
[5] Walker, S. A., Komistek, R., Hoff, W., and Dennis, D., 1996, "In-Vivo Pose Estimation of Artificial Knee Implants Using Computer Vision," *Proceedings of the 1996 33rd Annual Rocky Mountain Bioengineering Symposium & 33rd International ISA Biomedical Sciences Instrumentation Symposium*, Apr. 12–13, Colorado Springs, CO, Vol. 32, Instrument Society of America, Research Triangle Park, NC, pp. 143–150.
[6] Fukuoka, Y., Hoshino, A., and Ishida, A., 1997, "Accurate 3D Pose Estimation Method for Polyethylene Wear Assessment in Total Knee Replacement, *Proceedings of the 19th Annual International Conference of the IEEE Engineering in Medicine and Biology Society, Magnificent Milestones and Emerging Opportunities in Medical Engineering*, Oct. 30–Nov. 2, Chicago, IL, Vol. 4, IEEE, pp. 1810–1852.
[7] Zuffi, S., Leardini, A., Catani, F., Fantozzi, S., and Cappello, A., 1999, "A Model-Based Method for the Reconstruction of Total Knee Replacement Kinematics," IEEE Trans. Med. Imaging, **18**(10), pp. 981–991.
[8] You, B., Siy, P., Anderst, W., and Tashman, S., 2001, "In Vivo Measurement of 3-D Skeletal Kinematics From Sequences of Biplane Radiographs: Application to Knee Kinematics," IEEE Trans. Med. Imaging, **20**(6), pp. 514–525.
[9] Komistek, R. D., Dennis, D. A., and Mahfouz, M., 2003, "In Vivo Fluoroscopic Analysis of the Normal Human Knee," Clin. Orthop. Relat. Res., **410**, pp. 69–81.
[10] Li, G. A., Wuerz, T. H., and DeFrate, L. E., 2004, "Feasibility of Using Orthogonal Fluoroscopic Images to Measure In Vivo Joint Kinematics," J. Biomech. Eng., **126**(2), pp. 314–318.
[11] Suggs, J., Hanson, G., Durbhakula, S., Papannagari, R., Johnson, T., Freiberg, A., Rubash, H., and Li, G., 2005, "Patient Specific 3D Analysis of In Vivo Knee Kinematics After Cruciate Retaining Total Knee Arthroplasty," *Transactions From the 51st Annual Meeting of the ORS*, Washington, DC, Vol. 30, Orthopaedic Research Society.
[12] Canny, J., 1986, "A Computational Approach to Edge-Detection," IEEE Trans. Pattern Anal. Mach. Intell., **8**(6), pp. 679–698.
[13] Gronenschild, E., 1997, "The Accuracy and Reproducibility of a Global Method to Correct for Geometric Image Distortion in the X-Ray Imaging Chain," Med. Phys., **24**(12), pp. 1875–1888.
[14] Lee, E., 1989, "Choosing Nodes in Parametric Curve Interpolation," Comput.-Aided Des., **21**(6), pp. 363–370.
[15] Fletcher, R., 1987, *Practical Methods of Optimization*, 2nd ed, Wiley, Chichester, New York, p. 436.
[16] Short, A., Gill, H., Marks, B., Waite, J., Kellett, C., Price, A., O'Connor, J., and Murray, D., 2005, "A Novel Method for In Vivo Knee Prosthesis Wear Measurement," J. Biomech., **38**(2), pp. 315–322.
[17] Yamazaki, T., Watanabe, T., Nakajima, Y., Sugamoto, K., Tomita, T., Yoshikawa, H., and Tamura, S., 2004, "Improvement of Depth Position in 2-D/3-D Registration of Knee Implants Using Single-Plane Fluoroscopy," IEEE Trans. Med. Imaging, **23**(5), pp. 602–612.
[18] Li, G., DeFrate, L., Sun, H., and Gill, T., 2004, "In Vivo Elongation of the Anterior Cruciate Ligament and Posterior Cruciate Ligament During Knee Flexion," Am. J. Sports Med., **32**(6), pp. 1415–1420.
[19] DeFrate, L., Sun, H., Gill, T., Rubash, H., and Li, G., 2004, "In Vivo Tibiofemoral Contact Analysis Using 3D MRI-Based Knee Models," J. Biomech., **37**(10), pp. 1499–1504.
[20] Asano, T., Akagi, M., Tanaka, K., Tamura, J., and Nakamura, T., 2001, "In Vivo Three-Dimensional Knee Kinematics Using a Biplanar Image-Matching Technique, Clin. Orthop. Relat. Res., **388**, pp. 157–166.
[21] Koelzow, T., and Krueger, L., 2002, "Matching of a 3D Model Into a 2D Image Using a Hypothesize and Test Alignment Method," *Proceedings of the SPIE - The International Society for Optical Engineering: Advanced Signal Processing Algorithms, Architectures, and Implementations XII*, July 9–11, F. T. Luk, ed., SPIE, Bellingham, WA, Vol. 4791, pp. 222–232.
[22] Garling, E., Kaptein, B., Geleijns, K., Nelissen, R., and Valstar, E., 2005, "Marker Configuration Model-Based Roentgen Fluoroscopic Analysis," J. Biomech., **38**(4), pp. 893–901.
[23] Lavallee, S., and Szeliski, R., 1995, "Recovering the Position and Orientation of Free-Form Objects From Image Contours Using 3D Distance Maps," IEEE Trans. Pattern Anal. Mach. Intell., **17**(4), pp. 378–390.
[24] Mahfouz, M., Hoff, W., Komistek, R., and Dennis, D., 2003, "A Robust Method for Registration of Three-Dimensional Knee Implant Models to Two-Dimensional Fluoroscopy Images," IEEE Trans. Med. Imaging, **22**(12), pp. 1561–1574.
[25] Mahfouz, M., Hoff, W., Komistek, R., and Dennis, D., 2005, "Effect of Segmentation Errors on 3D-to-2D Registration of Implant Models in X-Ray Images," J. Biomech., **38**(2), pp. 229–239.
[26] Kaptein, B., Valstar, E., Stoel, B., Rozing, P., and Reiber, J., 2003, "A New Model-Based RSA Method Validated Using CAD Models and Models From Reversed Engineering," J. Biomech., **36**(6), pp. 873–882.
[27] Sato, T., Koga, Y., and Omori, G., 2004, "Three-Dimensional Lower Extremity Alignment Assessment System: Application to Evaluation of Component Position After Total Knee Arthroplasty," J. Arthroplasty, **19**(5), pp. 620–628.
[28] Valstar, E., de Jong, F., Vrooman, H., Rozing, P., and Reiber, J., 2001, "Model-Based Roentgen Stereophotogrammetry of Orthopaedic Implants," J. Biomech., **34**(6), pp. 715–722.
[29] Kaptein, B., Valstar, E., Stoel, B., Rozing, P., and Reiber, J., 2004, "Evaluation of Three Pose Estimation Algorithms for Model-Based Roentgen Stereophotogrammetric Analysis," Proc. Inst. Mech. Eng., Part H: J. Eng. Med., **218**(H4), pp. 231–238.